Catalytic Hydrothermal Upgrading of α-Cellulose using Iron Salts as a Lewis Acid

Sharifah Bee Abd Hamid,* Swe Jyan Teh, and You Sing Lim

The catalytic hydrothermal carbonization (C-HTC) method is proposed as a way to convert renewable feedstocks into carbon nanomaterial, using α-cellulose as the model compound. In this study, cellulose reacted with a controlled amount of Lewis acid catalyst ($FeCl_2$ and $FeCl_3$) under hydrothermal conditions, at temperatures ranging from 180 to 220 °C, for 6 to 24 h. The Lewis acid catalyst's effect on the formation of carbon nanomaterials in the C-HTC reaction was investigated. This study showed that Lewis acid catalysts promoted the complete carbonization of cellulose at a reduced temperature of 200 °C. The addition of $FeCl_2$ in C-HTC also promoted greater C=O functionality compared to $FeCl_3$. Furthermore, the surface area of the carbon nanomaterials derived from the hydrothermal carbonization of cellulose increased from 7.92 to 15.87 and 12.96 m^2 g^{-1} for the uncatalysed, $FeCl_2$ and $FeCl_3$-catalysed HTC, respectively. The findings in this study shed light on the effect of Lewis acid properties on the tunability of functional groups in the preparation of carbonaceous materials for high-end applications.

Keywords: Hydrothermal carbonization; Cellulose; Lewis acid catalyst; Heterogeneous catalysis

*Contact information: Nanotechnology & Catalysis Research Centre (NANOCAT), IPS Building, University Malaya, 50603, Kuala Lumpur, Malaysia; *Corresponding author: sharifahbee@um.edu.my*

INTRODUCTION

Biocarbon is a solid, carbon-rich material, derived from organic matter that has undergone a carbonization process. Biocarbon can be used in a wide variety of applications, due to its advantageous physical and chemical properties. For example, the high surface area and non-toxic nature of biocarbon make it suitable as an adsorbent for wastewater treatment (Singanan and Peters 2013; Mohan *et al.* 2014) and pollutant removal (Liu and Zhang 2009; Han *et al.* 2013). The calorific value of biocarbon is similar to that of lignite, making it an attractive substitute in the coal energy sector (Liu *et al.* 2012; Hribernik *et al.* 2013). Additionally, carbon-rich nanomaterials, which possess the appropriate functionality, can act as a catalyst or catalyst support through specific interactions between its surface and the surrounding reactants (Ding *et al.* 2012; Kalyani *et al.* 2013; Zhu *et al.* 2013).

From an agricultural standpoint, lignocellulosic biomass waste has often been utilised as a viable carbon feedstock for the production of biocarbon (Antal Jr. *et al.* 2007; Funke and Ziegler 2010; Jamari and Howse 2012). Bio-feedstock is typically comprised of three components: lignin, hemicelluloses, and cellulose. Cellulose, a straight chain polymer that consists of poly-glucose units, is the simplest and most ordered of the structures. Hemicellulose contains many different sugar monomers, such as xylose, fructose, and sucrose, while lignin consists of phenylpropane units with hydrophobic and aromatic properties, cross-linked in a complex, three-dimensional biopolymer structure (McKendry

2002; Titirici and Antonietti 2010). When lignocellulosic biomaterials undergo the carbonization process, bond cleavage and carbon-ring rearrangements occur so that the final product achieves a higher graphitic order. The energy requirement for the carbonization process increases from cellulose to hemicellulose to lignin, due to the increasing complexity in the structure of the components (Hosoya *et al.* 2007; Yang *et al.* 2007).

The carbonization process itself is the thermochemical conversion of organic material into a fixed carbon material. Presently, the carbonization of agricultural lignocellulosic biomass waste is carried out *via* pyrolysis. Various pyrolysis configurations have been used to yield useful products from the lignocellulosic biomass. When biomass is heated at high temperatures and subjected to a short retention time, in the absence of air (a process known as fast pyrolysis), bio-oil and biocarbon are produced as its major and minor products, respectively (Stefanidis *et al.* 2014). The heating of biomass under high temperatures for prolonged retention times is referred to as slow pyrolysis. Depending on lignin content of the precursor, the yield for the slow pyrolysis ranges from 24 to 46% wt. (Lee *et al.* 2013). The disadvantage of pyrolysis is that the process suffers from low yields and is intolerant of high water content. Thus, additional energy is required to dry the materials before pyrolysis.

Alternatively, the hydrothermal carbonization (HTC) process is a promising route to synthesize functional biocarbon with the desirable functional group (aldehyde, hydroxyl, carbonyl, carboxylic, *etc*.) for specific applications such as electrodes, supercapacitors, and gas storage media. The sustainable HTC system uses renewable lignocellulosic bio-resources and requires a relatively mild temperature to produce carbon nanomaterials with specific functionalities (Libra *et al.* 2011). The use of heated, pressurized water as solvent allows carbonization reactions to proceed at mild temperature conditions ranging from 180 to 250 °C (Titirici and Antonietti 2010). Hydrothermal carbonization is an attractive option because of its relatively simple and green technique, and it is scalable for the mass production of various carbon materials. When lacking a catalyst, HTC yields low-rank coal, and increasing the temperature results in a decrease of the C:O ratio (Libra *et al.* 2011). The addition of catalysts is expected to further improve the HTC process by reducing both the energy requirement and processing time.

Lewis acids such as metal salts, *e.g.* zinc chloride (Fechler *et al.* 2013), copper(II) acetate (Yu *et al.* 2004), and $[Fe(NH_4)_2(SO_4)_2]\cdot 6H_2O$ (Cui *et al.* 2006) have been considered as an alternative to mineral acids due to the greater ease in recovery of the metal salts, making the catalysed carbonization process more environmentally friendly. However, to the best of our knowledge, the effect of metal oxidation states in the catalysis of hydrothermal carbonization has not yet been explored. Furthermore, iron catalysts have not yet been applied in the catalyzed hydrothermal carbonization of higher level polysaccharides, *e.g.* cellulose. Therefore, this study was carried out to compare the catalytic activity between Fe^{2+} and Fe^{3+} ions in the hydrothermal carbonization of cellulose.

A one-pot catalytic-HTC (C-HTC) technique was proposed to prepare the functionalized biocarbon in the presence of different Lewis acid catalyst loading. Therefore, the present study was carried out to optimize the catalysis platform to convert cellulose into carbon-rich functional nanomaterials. This study evaluates the influence of divalent and trivalent Lewis acids on the C-H, C-O, and C-C bonds in cellulose during the HTC process.

EXPERIMENTAL

Materials

The carbon feedstock used in this experiment was α-cellulose (Sigma Aldrich, USA), which is a model compound of lignocellulosic bio-resources. For the catalysis reaction, divalent ($FeCl_2$, 99.5%, Merck, Germany) and trivalent ($FeCl_3$, 99.5%, Merck, Germany) iron chloride salts were employed as the Lewis acid catalyst.

Methods

Synthesis

Employing typical preparation techniques, 3 g of α-cellulose was dispersed into 50 mL of de-ionized water. A controlled amount (33.33 wt. %) of the catalyst was added to the cellulose solution and stirred until it was homogeneously mixed. The prepared solution was subsequently transferred into a Teflon-lined autoclave (80 mL) and heated at temperatures ranging from 180 to 220 °C for intervals varying between 6 and 24 h, as listed in Table 1. The ratio of catalyst to feedstock was altered in this experiment. The resulting carbon nanomaterials were washed several times with 10% wt. hydrochloric acid (HCl) to remove residue inorganic salts, then subsequently washed with de-ionized water until a neutral pH was obtained (Xiao *et al.* 2012). The purpose of the acid wash was to reduce the residue catalyst trapped in the formed carbon nanomaterials.

Characterization

Several characterization techniques were used to identify the resulting carbon products. The presence of functional groups in the final samples was investigated using Fourier transform infrared spectroscopy (Bruker IFS 66V/S, USA) and Raman spectroscopy (Renishaw inVia Raman microscope, UK), with ranges of 400 to 4000 cm^{-1} and 200 to 3200 cm^{-1}, respectively.

Sample crystallinity was investigated by X-ray diffraction (Bruker S4 Explorer, USA), with a powder diffractometer using Cu Kα radiation sources of 40 kV in the 2θ ranging from 20° to 70°. The chemical composition of the carbon products was characterized using a CHNOS (carbon, hydrogen, nitrogen, oxygen, sulfur) elemental analyzer (LECO TruSpec Micro CHNS, USA).

The surface morphology and size of final products were characterized using a field emission scanning electron microscope (FE-SEM) (Zeiss SUPRA 35VP; Germany). To determine the stability of the catalyst, the leaching test was performed by dispersing 0.1 g of the sample in 100 mL distilled water. This dispersion was sealed and stirred for 72 h. The dispersed carbon was then separated by means of centrifugation and followed by passing the supernatant through a 0.22 µm syringe filter. The liquid was then analysed for the presence of Fe and Cl using methods APHA 3120B, 20th Edition 1998 and APHA 4110 D, respectively.

The BET Surface area, pore volume and pore size distribution of the samples were analysed with a TriStar II Surface Area and Porosity Analyzer. The samples were outgassed under vacuum at 200 °C for 5 h to remove moisture content before conducting the nitrogen gas adsorption method. Surface area and pore diameter was calculated by Brunauer-Emmett-Teller (BET) method, whereas micropore volume was obtained by the t-plot method.

RESULTS AND DISCUSSION

The CHNOS elemental analysis determines the organic content of an unknown sample. A smaller H/C ratio indicates high graphitic structure in the analyte. Other studies have reported a carbon content of around 60 to 70% wt (Sevilla and Fuertes 2009; Baccile *et al.* 2010; Braghiroli *et al.* 2014). During this study, the product yield was between 62 and 66% wt. for the uncatalyzed samples, whereas catalyzed HTC cellulose yielded between 66 and 73% wt. Each sample was prepared in duplicate, and the average value with standard deviation values are reported in Table 1. In all samples, the carbon content increased as the temperature increased, subsequently decreasing the H/C ratio (Table 1). This indicates increasing effectiveness of carbonization at higher temperatures. There is a sharp increase in the carbon content between cellulose carbonized at 180 and 200 °C, which is in agreement with the previous works conducted by Falco *et al.* (2011). This indicates that cellulose undergoes significant structural disruption when subjected to a reaction temperature of 200 °C and onwards, thus opening up more reactive sites for the dehydration and aromatization reactions. In this study, the oxidation state of the catalyst plays a mildly significant role towards increasing the carbon content of the HTC treated cellulose, as shown by the relatively higher carbon content of the $FeCl_2$-catalyzed samples.

Table 1. Reaction Conditions and Chemical Elemental Analysis for Carbon Nanomaterials Obtained from C-HTC of Cellulose Feedstock

No	Temp. (°C)	Reaction time (hours)	Uncatalyzed				$FeCl_2$-catalyzed				$FeCl_3$-catalyzed			
			C [wt.] (SD)	H [wt.] (SD)	H/C [at.]	Yield [%]	C [wt.] (SD)	H [wt.] (SD)	H/C	Yield [%]	C [wt.] (SD)	H [wt.] (SD)	H/C [at.]	Yield [%]
A1	180	12	64.03 (0.08)	4.79 (0.09)	0.90	62.0	67.94 (2.03)	4.86 (0.02)	0.86	66.4	67.02 (0.16)	4.98 (0.01)	0.89	64.3
A2		24	65.98 (1.56)	4.90 (0.15)	0.89	63.5	69.75 (0.77)	4.54 (0.12)	0.78	69.8	69.01 (0.12)	4.84 (0.16)	0.84	68.6
B1	200	12	66.55 (0.45)	4.68 (0.02)	0.84	65.0	74.08 (0.22)	4.48 (0.24)	0.73	72.3	73.32 (0.24)	4.61 (0.42)	0.75	70.2
B2		24	68.23 (0.31)	4.61 (0.11)	0.81	64.7	72.96 (0.63)	4.34 (0.01)	0.71	73	74.58 (1.03)	4.59 (0.08)	0.74	71.0
C1	220	12	69.20 (0.48)	4.64 (0.04)	0.8	66.5	72.50 (0.09)	4.23 (0.12)	0.70	72.8	72.58 (0.33)	4.44 (0.12)	0.73	72.5
C2		24	70.70 (1.86)	4.60 (0.01)	0.78	66.8	73.66 (0.11)	4.18 (0.09)	0.68	73.5	73.90 (0.31)	4.58 (0.38)	0.74	72.9

The FT-IR spectra of HTC carbon nanoparticles, recorded in the frequency range of 400 to 4000 cm^{-1}, showed a very broad band at 3400 cm^{-1} that resulted from the vibrating bands of hydroxyl groups and the stretched vibrations of the adsorbed water molecules (Fig. 1). The intensity of absorption in the IR spectrum is related to the change in the dipole moment that occurs during the vibration. There are several bands which reveal the presence of various surface functionalities and aromatic rings in the samples. The IR spectra of the catalyst recorded a medium absorption of 1701 cm^{-1}, which can be attributed to the

carbonyl (C=O) group. The presence of aromatic rings is evidenced by the weak band in the 750 to 875 cm^{-1} region, which corresponds to the aromatic C-H out of plane bending. Additionally, the medium intensity peak observed at 1620 cm^{-1} indicates aromatic C=C vibrations (Kang *et al.* 2012; Zhang *et al.* 2015). These samples also possess an aliphatic C-H structure at 2800 to 3000 cm^{-1}, which can be attributed to the aliphatic stretching as well as spectra in the 1000- to 1460-cm^{-1} region, corresponding to the C-O stretching in hydroxyl, ester or ether, and O-H bending vibrations (Presser *et al.* 2011). For the uncatalyzed samples, the intensity of aliphatic structure was high, in the 1000- to 1460-cm^{-1} region. For the catalyzed samples, there was a considerable reduction in the area of the strong band at 1000 to 1460 cm^{-1}. It can be seen in Fig. 1 that the area of this band is smaller for the catalyzed HTC in comparison to the uncatalyzed HTC. Meanwhile, the IR spectrum representing the aromatic structures at 1620 cm^{-1} arises, indicating that the aromatization process takes place during C-HTC (Falco *et al.* 2011). Additionally, samples catalyzed by $FeCl_2$ show a greater amount of C=O functionality, as well as C=C aromatic compound, as shown by the stronger absorption at these bands in comparison to $FeCl_3$ and uncatalyzed HTC.

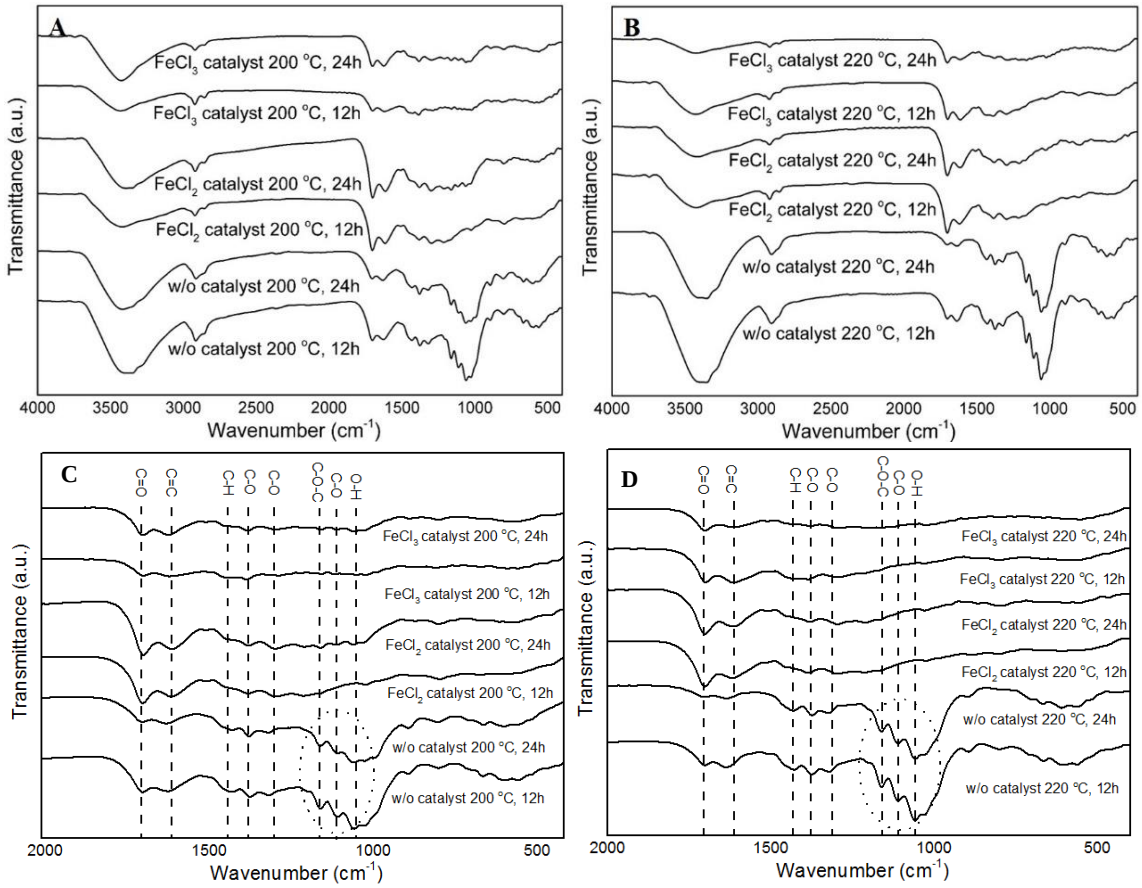

Fig. 1. FT-IR spectra analysis of the synthesized samples at different conditions: (a) 200 °C, 12 and 24 h, (b) 220 °C, 12 h and 24 h. Further magnification of graphs (a) and (b) in the 2000-500 cm^{-1} region are shown in (c) and (d), respectively.

Raman spectroscopy is an analytical technique that detects changes in polarisability, and it is a complementary technique to FT-IR. Raman scattering is a phenomenon in which inelastic light scatters due to symmetrical bond vibration. Usually,

Raman spectroscopy of amorphous carbon materials indicates characteristic peaks of 1300 cm^{-1} and 1590 cm^{-1}, referring to D band and G band, respectively. In this study, the G bands of the samples indicate the E_{2g2} mode of graphite, sp^2 C=C stretching ability, or a combination of both (Schwan *et al.* 1996). Furthermore, as shown in Fig. 2, these G bands were typically broad. The peak broadening could be a result of cluster size, indicating larger particles. Raman analysis is able to check for the presence of aromatic structures in the samples by analyzing the intensity of the G band. Higher intensity of the G band indicates higher sp^2 C=C content, an aromatic structure. Interestingly, it was found that D bands were absent from the Raman spectrum of the $FeCl_2$- and $FeCl_3$-catalyzed cellulose HTC, indicating the absence of sp^3 carbon disorders in the samples. The degree of aromatization for both divalent- and trivalent-Fe catalyzed samples is similar. However, samples treated with $FeCl_2$ catalysts exhibit slightly higher intensities of the G band when compared to the trivalent-Fe sample, for samples undergoing 24-h reactions.

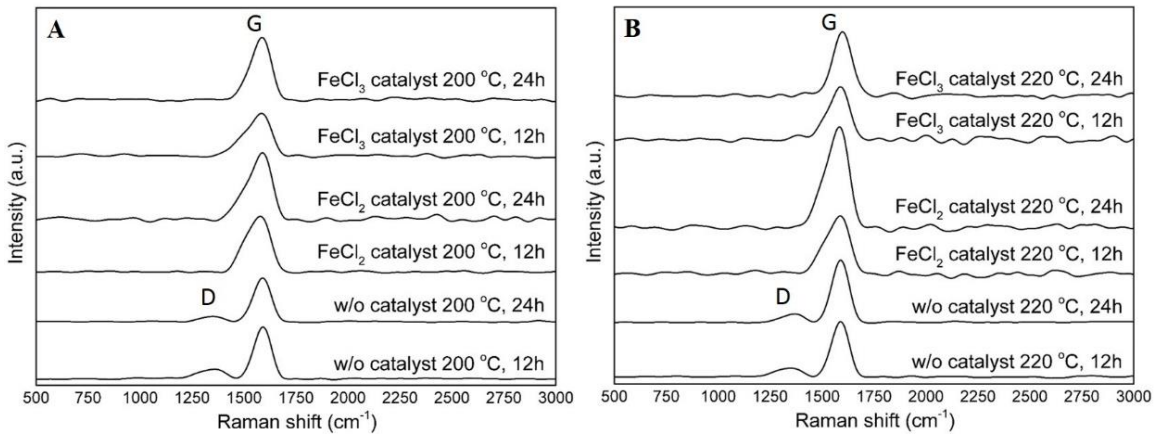

Fig. 2. Raman spectroscopy analysis of the synthesized samples at different conditions: (a) 200 °C, 12 and 24 h, (b) 220 °C, 12 h and 24 h

X-ray diffraction (XRD) analysis shows the degree of crystallinity of the synthesized nanomaterials. The XRD analysis employed Cu kα radiation at 2θ, ranging from 10^o to 80^o for every gram of the sample. The results in Fig. 3 show that the products of the uncatalyzed HTC exhibited three characteristic peaks at (101) reflection at $2\theta = 15^o$, (002) reflection at $2\theta = 22.5^o$, and (040) at $2\theta = 34^o$ (Sevilla and Fuertes 2009). The (101) and (002) reflections correspond to the transversal arrangement of the crystallites in cellulose, while the (040) reflection is caused by the longitudinal structure of the polymer. The appearance of these peaks indicates that the uncatalyzed samples did not undergo a complete conversion of cellulose to carbon, thus leaving some properties of cellulose in the sample. For samples synthesized with the aid of $FeCl_2$ and $FeCl_3$ catalysts, the characteristic peaks of cellulose disappeared. The results obtained show that the catalyzed samples were in an amorphous state, suggesting that the crystalline phase of cellulose was broken during carbonization. The catalytic activity of $FeCl_2$ and $FeCl_3$ altered the carbonization process by improving the cracking rate of the cellulose bonding. In comparing the effects of divalent and trivalent iron chloride, it was found that both catalysts were able to aid in the formation of amorphous carbon at different reaction temperatures and residence times. However, one result highlighted that the Fe^{2+} ion had the stronger catalyst effect at higher temperatures. By observing the XRD pattern for HTC cellulose reaction at 220 °C for 12 h, the Fe^{2+} catalyzed samples exhibited more amorphous

characteristics when compared to the Fe^{3+} catalyzed samples. Therefore, these patterns justify that divalent Lewis acid catalysts were the better catalyst for the cleavage of glycosidic bonds at higher temperature. For samples synthesized for 12 and 24 h, all samples followed similar trends, with no significant evidence to prove that the reaction proceeding for 12 h was better than the reaction for 24 h.

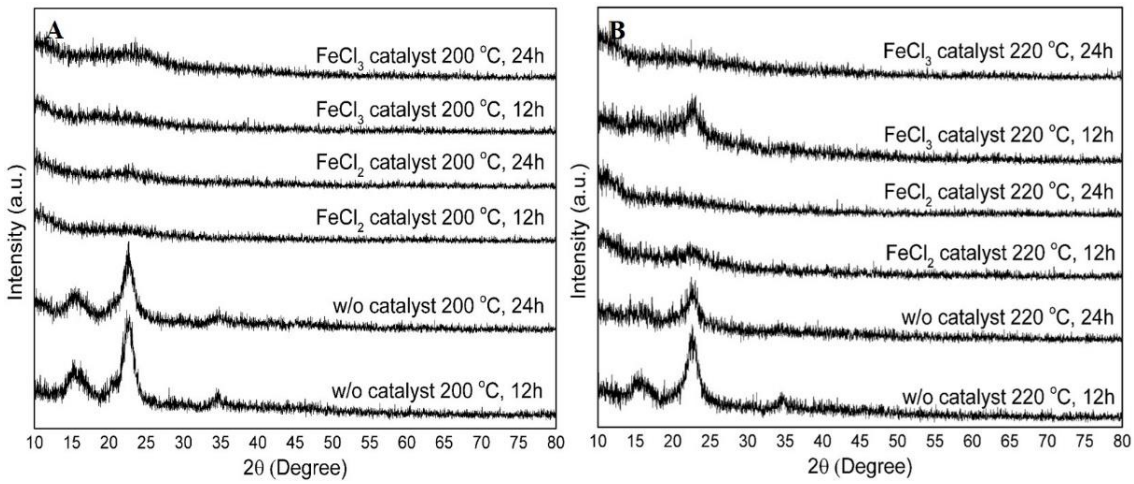

Fig. 3. XRD analysis of the synthesized samples at different reaction conditions (a) 200 °C, 12 and 24 h, (b) 220 °C, 12 and 24 h

Scanning electron microscope (SEM) characterization reveals the samples' surface morphology and particle size. From the SEM images, the uncatalyzed samples obtained by hydrothermal treatment for 12 h at 220 °C show that the morphology of the samples was mostly irregular, with limited micro-sized carbon spheres (Fig. 4a). The sample displayed carbon microspheres with particle size distribution ranging from 2 to 3 µm. Fig. 4a supports the evidence from XRD analyses whereby uncatalyzed samples did not undergo complete carbonization.

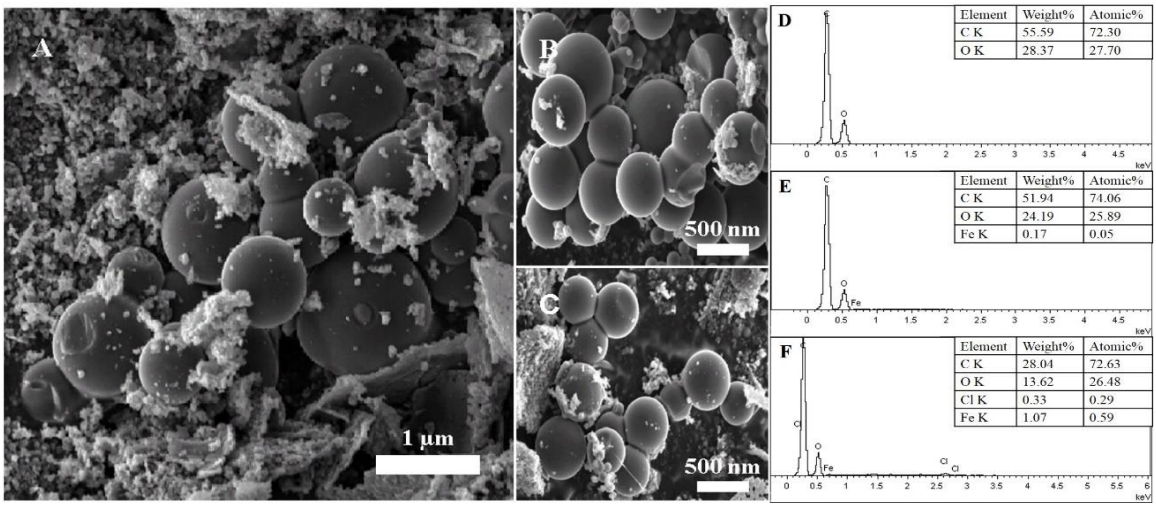

Fig. 4. SEM images of the synthesized samples at 220 °C, 12 h: (a) uncatalyzed sample, (b) $FeCl_2$ catalyzed sample, and (c) $FeCl_3$ catalyzed sample. EDX measurements of carbon nanomaterials synthesized from cellulose (d) without catalyst, (e) with $FeCl_2$ catalyst and (f) with $FeCl_3$ catalyst.

Comparing the SEM images of Fe^{2+} and Fe^{3+} catalyzed samples obtained at similar reaction conditions, carbonaceous nanomaterials were formed under Lewis acid-catalyzed conditions. Aggregated, uniform nano-spheres were formed with particle diameters ranging from 300 to 600 nm (Figs. 4b and 4c). However, some irregularly shaped particles can still be seen from the SEM image of Fe^{3+}-catalyzed sample (Fig. 4c). It is possible that the trivalent Fe has lower accessibility to aid the hydrothermal carbonization of cellulose. Furthermore, the present results suggest that the $FeCl_2$ catalyst possesses higher catalytic severity for the cracking of cellulose bonds during the carbonization of cellulose, leading to higher-quality carbon nanomaterials.

Energy dispersive X-ray (EDX) spot analysis of the samples determined the composition of C and O elements at the surface of the synthesized samples. Compared to the uncatalysed sample (Fig. 4d), the C content of the hydrochar increased in the presence of catalyst. More specifically, the composition of C was slightly higher for the $FeCl_2$-catalyzed HTC (Fig. 4e) than the $FeCl_3$-catalyzed HTC (Fig. 4f), corresponding with the CHO elemental analysis. Minimal Fe was present in the samples (< 0.59%) with little effect on the elemental composition, indicating the facile removal of catalyst from the samples upon rinsing with hydrochloric acid and deionized water.

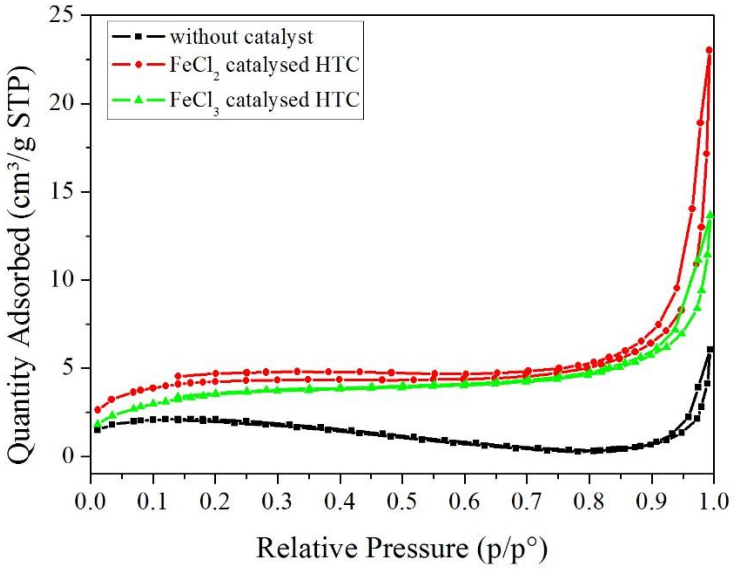

Fig. 5. Brunauer-Emmett-Teller (BET) adsorption isotherm of the uncatalysed, $FeCl_2$ and $FeCl_3$-catalysed samples at 220 °C, 12 h

It was observed that the adsorption isotherm contained three characteristic regions: (a) the initial part of the curve with a gentle rise resulted from nitrogen uptake at $P/P^o < 0.1$; (b) the second part that is the plateau of the curve between $0.1 < P/P^o < 0.9$ and (c) the upward bend of the curve at the last region when equilibrium was reached ($P/P^o \approx 0.9$).

The characteristics of the curve indicated a Type II isotherm. The shape of the isotherm indicated the presence of a high proportion of micropores with some contribution of meso and macropores (Chowdhury *et al.* 2012). The aforementioned surface analysis determined that the average pore diameter of the carbon nanomaterials derived from uncatalysed HTC of cellulose was 47 Å. The addition of Fe^{2+} and Fe^{3+} catalyst increased the pore diameter to 89 and 65 Å, respectively, which may be attributed to the formation of additional pores after the removal of catalyst *via* acid washing. Nevertheless, the surface

area of carbon nanomaterials derived from the hydrothermal carbonization of cellulose increased from 7.92 to 15.87 and 12.96 m^2 g^{-1} for the uncatalysed, $FeCl_2$ and $FeCl_3$-catalysed HTC, respectively.

Results obtained from surface area analysis of the carbon nanomaterials derived from uncatalysed and catalysed HTC are summarised in Table 2.

Table 2. Physico-chemical Characteristics of Carbon Nanomaterials Derived from Uncatalysed, $FeCl_2$- and $FeCl_3$-catalysed C-HTC of Cellulose at 220 °C, 12 hours' Reaction Time

Physico-chemical characteristics	uncatalysed	$FeCl_2$-catalysed	$FeCl_3$-catalysed
BET surface area	7.9205 m^2 g^{-1}	15.8722 m^2 g^{-1}	12.9626 m^2 g^{-1}
t-plot micropore surface area	7.4177 m^2 g^{-1}	8.3520 m^2 g^{-1}	1.7809 m^2 g^{-1}
Average pore diameter	47.3879 Å	89.6985 Å	65.2252 Å

Mineral acids, *e.g.* sulphuric acid, phosphoric acid, and hydrochloric acid, have been traditionally used to accelerate the carbonization process by accelerating the dehydration reaction to form carbon basic structural units (BSU) before the recondensation occurs to form carbonaceous particles, *i.e.* hydrochar. Many reports have been found on the carbonization of simple sugars. In the presence of acid, simple sugars are reduced to furfural and 5-HMF (Sevilla and Fuertes 2009). The production of 5-HMF also was observed with good yield from fructose, sucrose, and xylose (Tong *et al.* 2011; Choudhary *et al.* 2012).

Alternatively, Fe anions, being electron acceptors, *i.e.* Lewis acids, can also potentially catalyse the dehydration process by electrophilic attack on the glycosidic bond in the cellulose structure. Previously, $[Fe(NH_4)_2(SO_4)_2]\cdot 6H_2O$ has been used as a catalyst in the carbonization of glucose, which led to the fabrication of hollow carbonaceous microspheres (Cui *et al.* 2006).

In this study, the presence of a catalyst allowed the effective carbonization at temperatures as low as 200 °C, whereas previously a minimum temperature of 220 °C was necessary to decompose the cellulose chains, under uncatalysed conditions (Sevilla and Fuertes, 2009). The sp^3 disorder was also reduced in the samples through the use of catalyst. Due to the complexity of the carbonization process, it was a challenge to pinpoint the exact role of catalyst in the carbonization process. It was proposed previously that the mechanism of carbonization includes a hydrolysis phase to break the cellulose chains into oligosaccharides (Sevilla and Fuertes 2009), followed by dehydration to form furan compounds (Xiao *et al.* 2012). The oligosaccharides, phenolic, and furan compounds then become repolymerized to form soluble chains. Subsequently, C=C bonds are produced via keto-enol tautomerization and intramolecular dehydration. When threshold conditions are achieved, carbon nuclei particles are formed and further crosslinking between these compounds lead to the growth in the carbon particles (Ryu *et al.* 2010).

It is possible that Lewis acid catalysts play multiple roles in accelerating the hydrolysis and aromatization reactions, leading to C-O bond cleavage and the formation of C=C bonds. Lewis acid catalysts were found to promote polymer crosslinking, graphitization, and hydrochar yield (Cai *et al.* 2007). Lewis acid catalysts are electron

acceptors, and the notion has been proposed to break bonds in the lignocellulosic structure *via* electrophilic attack on the C-H, C-O, or C-C bonds (Molina-Sabio and Rodriguez-Reinoso 2004).

From the data presented herein, one can see that there are subtle differences in the application of ionic charge on the hydrothermal carbonization of cellulose. It was observed that the C=O group was still significantly present in the Fe^{2+}-catalysed samples. On the other hand, the higher acidic properties of the Fe^{3+} cation resulted in a more reduced form of carbon, indicated by the diminished peak at 1700 cm^{-1}, which corresponds with the carbonyl, C=O group. Leaching test was performed and it did not show a detectable amount of Fe content in the sample. Thus there is no chance of introducing Fe as a secondary pollutant in the process stream when using the hydrochar prepared here.

CONCLUSIONS

1. The results show that the addition of Fe-salts promotes the synthesis of carbonaceous products from cellulose. This study shows that the carbonization of cellulose is incomplete at 200 °C in the absence of the iron salt; however, with the aid of Lewis acid catalysts, complete carbonization was observed.
2. The addition of $FeCl_2$ in C-HTC promoted greater C=O functionality compared to $FeCl_3$. The stable oxidation state of Fe^{3+} ions reduced the oxidation of carbon functional groups.
3. BET analysis showed that adding Fe containing salt can act as catalyst to enhance the surface area substantially.

ACKNOWLEDGMENTS

The authors wish to express their thanks to the University of Malaya for their financial support through HIR grant (H-21001-F0032) for their financial support.

REFERENCES CITED

Antal Jr., M. J., Wade, S. R., and Nunoura, T. (2007). "Biocarbon production from Hungarian sunflower shells," *J. Anal. Appl. Pyrol.* 79(1-2), 86-90. DOI: 10.1016/j.jaap.2006.09.005

Baccile, N., Antonietti, M., and Titirici, M.-M. (2010). "One-step hydrothermal synthesis of nitrogen-doped nanocarbons: Albumine directing the carbonization of glucose," *ChemSusChem* 3(2), 246-253. DOI: 10.1002/cssc.200900124

Braghiroli, F. L., Fierro, V., Izquierdo, M. T., Parmentier, J., Pizzi, A., and Celzard, A. (2014). "Kinetics of the hydrothermal treatment of tannin for producing carbonaceous microspheres," *Bioresource Technology* 151, 271-277. DOI: 10.1016/j.biortech.2013.10.045

Cai, Y., Hu, Y., Song, L., Xuan, S., Zhang, Y., Chen, Z., and Fan, W. (2007). "Catalyzing carbonization function of ferric chloride based on acrylonitrile–butadiene–styrene copolymer/organophilic montmorillonite nanocomposites,"

Polymer Degradation and Stability 92(3), 490-496. DOI: 10.1016/j.polymdegradstab.2006.08.029

Choudhary, V., Sandler, S. I., and Vlachos, D. G. (2012). "Conversion of xylose to furfural using Lewis and Brønsted acid catalysts in aqueous media," *ACS Catalysis* 2(9), 2022-2028. DOI: 10.1021/cs300265d

Chowdhury, Z. Z., Zain, S. M., Khan, R. A., Arami-Niya, A., and Khalid, K. (2012). "Process variables optimization for preparation and characterization of novel adsorbent from lignocellulosic waste," *BioResources* 7(3), 3732-3754.

Cui, X., Antonietti, M., and Yu, S. H. (2006). "Structural effects of iron oxide nanoparticles and iron ions on the hydrothermal carbonization of starch and rice carbohydrates," *Small* 2(6), 756-759. DOI: 10.1002/smll.200600047

Ding, Y., Li, J., Zhao, Y., and Guan, L. (2012). "Direct growth of $LiMn_2O_4$ on carbon nanotubes as cathode materials for lithium ion batteries," *Mater. Lett.* 68, 197-200. DOI: 10.1016/j.matlet.2011.10.090

Fechler, N., Wohlgemuth, S.-A., Jäker, P., and Antonietti, M. (2013). "Salt and sugar: Direct synthesis of high surface area carbon materials at low temperatures via hydrothermal carbonization of glucose under hypersaline conditions," *Journal of Materials Chemistry A* 1(33), 9418-9421. DOI: 10.1039/C3TA10674H

Falco, C., Baccile, N. and Titirici, M. M. (2011). "Morphological and structural differences between glucose, cellulose and lignocellulosic biomass derived hydrothermal carbons," *Green Chem.* 13(11), 3273-3281. DOI: 10.1039/C1GC15742F

Funke, A., and Ziegler, F. (2010). "Hydrothermal carbonization of biomass: A summary and discussion of chemical mechanisms for process engineering," *Biofuels Bioprod. Biorefin.* 4(2), 160-177. DOI: 10.1002/bbb.198

Han, Y., Boateng, A. A., Qi, P. X., Lima, I. M., and Chang, J. (2013). "Heavy metal and phenol adsorptive properties of biochars from pyrolyzed switchgrass and woody biomass in correlation with surface properties," *J. Env. Manag.* 118, 196-204. DOI: 10.1016/j.jenvman.2013.01.001

Hosoya, T., Kawamoto, H., and Saka, S. (2007). "Pyrolysis behaviors of wood and its constituent polymers at gasification temperature," *Journal of Analytical and Applied Pyrolysis* 78(2), 328-336. DOI:http://dx.doi.org/10.1016/j.jaap.2006.08.008

Hribernik, M., Anwar, A., Turkstra, A., and Zannini, M. C. (2013). "Potential of clean coal technology in India: An SME perspective," *European Business and Technology Centre*. http://www.ebtc.eu/pdf/130614_REP_Potential-of-clean-coal-technologies-in-India_An-SME-perspective_Web.pdf. Accessed 30 April 2014.

Jamari, S. S., and Howse, J. R. (2012). "The effect of the hydrothermal carbonization process on palm oil empty fruit bunch," *Biomass Bioenerg.* 47, 82-90. DOI: 10.1016/j.biombioe.2012.09.061

Kalyani, P., Anitha, A., and Darchen, A. (2013). "Activated carbon from grass - A green alternative catalyst support for water electrolysis," *Int. J. Hydrogen Energ.* 38(25), 10364-10372. DOI: 10.1016/j.ijhydene.2013.06.022

Kang, S., Li, X., Fan, J., and Chang, J. (2012). "Characterization of hydrochars produced by hydrothermal carbonization of lignin, cellulose, D-xylose, and wood meal," *Industrial & Engineering Chemistry Research* 51(26), 9023-9031.

Lee, Y., Park, J., Ryu, C., Gang, K. S., Yang, W., Park, Y. K., Jung, J., and Hyun, S. (2013). "Comparison of biochar properties from biomass residues produced by slow

pyrolysis at 500 °C," *Bioresource Technol.* 148, 196-201. DOI: 10.1016/j.biortech.2013.08.135

Libra, J. A., Ro, K. S., Kammann, C., Funke, A., Berge, N. D., Neubauer, Y., Titirici, M. M., Fühner, C., Bens, O., and Kern, J. (2011). "Hydrothermal carbonization of biomass residuals: A comparative review of the chemistry, processes and applications of wet and dry pyrolysis," *Biofuels* 2(1), 71-106. DOI: 10.4155/bfs.10.81

Liu, Z., and Zhang, F. S. (2009). "Removal of lead from water using biochars prepared from hydrothermal liquefaction of biomass," *J. Haz. Mat.* 167(1-3), 933-939. DOI: 10.1016/j.jhazmat.2009.01.085

Liu, Z., Quek, A., Kent-Hoekman, S., Srinivasan, M. P., and Balasubramanian, R. (2012). "Thermogravimetric investigation of hydrochar-lignite co-combustion," *Bioresource Technol.* 123, 646-652. DOI: 10.1016/j.biortech.2012.06.063

McKendry, P. (2002). "Energy production from biomass (part 1): Overview of biomass," *Bioresource Technol.* 83(1), 37-46. DOI: 10.1016/S0960-8524(01)00118-3

Mohan, D., Sarswat, A., Ok, Y. S., and Pittman Jr., C. U. (2014). "Organic and inorganic contaminants removal from water with biochar, a renewable, low cost and sustainable adsorbent – A critical review," *Bioresource Technol*. 160, 191-202. DOI: 10.1016/j.biortech.2014.01.120

Molina-Sabio, M., and Rodrıguez-Reinoso, F. (2004). "Role of chemical activation in the development of carbon porosity," *Colloid Surface A: Physicochemical and Engineering Aspects* 241(1), 15-25. DOI: 10.1016/j.colsurfa.2004.04.007

Presser, V., Heon, M., and Gogotsi, Y. (2011). "Carbide-derived carbons – From porous networks to nanotubes and graphene,"*Advanced Functional Materials* 21(5), 810-833. DOI: 10.1002/adfm.201002094

Ryu, J., Suh, Y. W., Suh, D. J., and Ahn, D. J. (2010). "Hydrothermal preparation of carbon microspheres from mono-saccharides and phenolic compounds," *Carbon* 48(7), 1990-1998. DOI: 10.1016/j.carbon.2010.02.006

Schwan, J., Ulrich, S., Batori, V., Ehrhardt, H., and Silva, S. (1996). "Raman spectroscopy on amorphous carbon films," *J Appl. Phys.* 80(1), 440-447. DOI: 10.1063/1.362745

Sevilla, M., and Fuertes, A. B. (2009). "The production of carbon materials by hydrothermal carbonization of cellulose," *Carbon* 47(9), 2281-2289. DOI: 10.1016/j.carbon.2009.04.026

Singanan, M., and Peters, E. (2013). "Removal of toxic heavy metals from synthetic wastewater using a novel biocarbon technology," *J. Env. Chem. Eng.* 1(4), 884-890. DOI: 10.1016/j.jece.2013.07.030

Stefanidis, S. D., Kalogiannis, K. G., Iliopoulou, E. F., Michailof, C. M., Pilavachi, P. A. and Lappas, A. A. (2014). "A study of lignocellulosic biomass pyrolysis via the pyrolysis of cellulose, hemicellulose and lignin," *J. Anal. Appl. Pyrol.* 105, 143-150. DOI: 10.1016/j.jaap.2013.10.013

Titirici, M. M., and Antonietti, M. (2010). "Chemistry and materials options of sustainable carbon materials made by hydrothermal carbonization," *Chem. Soc. Rev.* 39(1), 103-116. DOI: 10.1039/B819318P

Tong, X., Li, M., Yan, N., Ma, Y., Dyson, P. J., and Li, Y. (2011). "Defunctionalization of fructose and sucrose: Iron-catalyzed production of 5-hydroxymethylfurfural from fructose and sucrose," *Catalysis Today, 175*(1), 524-527. DOI:10.1016/j.cattod.2011.03.003

Xiao, L. P., Shi, Z. J., Xu, F., and Sun, R. C. (2012). "Hydrothermal carbonization of lignocellulosic biomass," *Bioresource Technol.* 118, 619-623. DOI: 10.1016/j.biortech.2012.05.060

Yang, H., Yan, R., Chen, H., Lee, D. H., and Zheng, C. (2007). "Characteristics of hemicellulose, cellulose and lignin pyrolysis," *Fuel* 86(12–13), 1781-1788. DOI: http://dx.doi.org/10.1016/j.fuel.2006.12.013

Yu, S.-H., Cui, X., Li, L., Li, K., Yu, B., Antonietti, M., and Cölfen, H. (2004). "From starch to metal/carbon hybrid nanostructures: Hydrothermal metal-catalyzed carbonization," *Advanced Materials* 16(18), 1636-1640. DOI: 10.1002/adma.200400522

Zhang, L., Wang, Q., Wang, B., Yang, G., Lucia, L. A., and Chen, J. (2015). "Hydrothermal carbonization of corncob residues for hydrochar production," *Energy & Fuels* 29(2), 872-876. DOI: 10.1021/ef502462p

Zhu, L. W., Zhou, L. K., Li, H. X., Wang, H. F., and Lang, J. P. (2013). "One-pot growth of free-standing CNTs/TiO_2 nanofiber membrane for enhanced photocatalysis," *Mater. Lett.* 95, 13-16. DOI: 10.1016/j.matlet.2013.01.004

Article resubmitted: June 5, 2014; Peer review completed: January 3, 2015; Revised version received and accepted: July 15, 2015; Published: August 3, 2015.
DOI: 10.15376/biores.10.3.5974-5986